[4Fe-4S]-mediated proton-coupled electron transfer enables the efficient degradation of chloroalkenes by reductive dehalogenases

Xuan Zhang,[†] Zikuan Wang,[§] Zhen Li,[†] Sason Shaik,[Δ,*] Binju Wang[†,*]

[†]State Key Laboratory Physical Chemistry of Solid Surfaces and Fujian Provincial Key Laboratory of Theoretical and Computational Chemistry, College of Chemistry and Chemical Engineering, Xiamen University, Xiamen 361005, P. R. China

[Δ]Institute of Chemistry, The Hebrew University of Jerusalem, 91904, Jerusalem, Israel

[§]Max-Planck-Institut für Kohlenforschung, Kaiser-Wilhelm-Platz 1, Mülheim an der Ruhr 45470, Germany

***KEYWORDS**: QM/MM, [4Fe-4S] cluster, PCET, Super-exchange enhancement; Reductive dehalogenase*

ABSTRACT: Reductive dehalogenases (RDases) are key enzymes involved in the degradation of organohalide compounds. Despite extensive experimental and computational studies, the catalytic mechanism of RDases remains unclear. We show here that the proximal $[4Fe\text{-}4S]^{1+}$ cluster of the reductive dehalogenase PceA can mediates a proton-coupled electron transfer (PCET) process to quench the substrate radical. Such $[4Fe\text{-}4S]^{1+}$-mediated PCET process is *enhanced by both exchange and super-exchange interactions.* The participation of $[4Fe\text{-}4S]^{1+}$ in mediating a PCET process in RDases is unexpected, though well known in reducing Co(II). In addition, in RDases the Arg305 residue acts as an efficient proton donor for the PCET reactions. The deprotonated Tyr246 serves to maintain the favorable conformation of Arg305 during catalysis, and sustains its proton donation ability, which is requested during the PCET reaction. Such a novel mechanism *enables the efficient detoxification of chloroalkene pollutants by the reductive dehalogenase PceA*. These results highlight the critical role of the proximal [4Fe-4S] 、

1.INTRODUCTION

Organohalides are widely used in agricultural, dyestuff, chemical, and pharmaceutical industries.[1] These compounds are usually toxic and can cause persistent environmental pollution. As such, nature has evolved several pathways for degradation of organohalogen compounds, including: a hydrolytic pathway utilized by haloalkane dehalogenases,[2,3] redox or non-redox pathways mediated by flavin-dependent dehalogenases,[4] an oxidative pathway mediated by heme-dependent dehaloperoxidase[5,6] and a reductive pathway mediated by reductive dehalogenases (RDases).[7-9]

RDases belong to the subfamily of cobalamin(B12)-dependent enzymes, which contain two [4Fe-4S] clusters capable of transporting the reduction equivalents during the catalytic reactions.[10] In particular, the closest [4Fe-4S] cluster is just 8.4 Å away from the Co center of cobalamin in the RDase PceA (Figure 1a), which enables an efficient electron transfer from the [4Fe-4S] cluster to the active site of the enzyme.[11,12] Unlike the hydrolytic enzymes which have a limited substrate scope, RDases can act on various haloalkenes, and reduce the corresponding C-X (X=Cl, Br) bonds to C-H bonds.[13,14] Thus, RDases are useful for the detoxification *of haloalkene pollutants such as perchloroethylene (PCE) and trichloroethene (TCE), which are widely used in dry cleaning*.

To date, a number of RDases including TmrA,[15,16] CfrA,[17,18] VcrA,[19,20] CbrA,[21,22] PceA[13,23-25] and NpRdhA[14,26] have been characterized. Among these, the well characterized PceA can catalyze the reductive dehalogenation of alkenyl chlorides and bromides.[13,23,27,28] A typical reaction of PceA involves the dechlorination of PCE, which can be successively dechlorinated to TCE and *cis*-dichloroethylene (DCE). As shown in Figure 1a, PceA has an amphiphilic active site on the β face of its corrin ring (PDB: 4UR0).[13] The hydrophilic residues Tyr246, Asn272, Arg305 are located on the left side of the substrate, while the hydrophobic residues Phe38 and Trp376 are situated on the right side.

It is recognized that the enzymatic dechlorination of PCE by PceA is initiated by the reduction of Co(II) to the reduced Co(I)-state of cobalamin (Figure 1b).[13,14] The following dechlorination reactions involve two separate electron transfers (Figure 1b). While one electron could be donated by the reduced Co(I), *the origins of the second electron transfer is still unresolved*. Given that the [4Fe-4S] cluster is in close proximity to the substrate, the second electron could be donated by [4Fe-4S] cluster via an outer-sphere mechanism. In addition, the identity of the proton source for the formation of the new C-H bond is being debated.[13,29] It is unclear if the proton is supplied by the protonated Tyr246[13,23,30] or another residue.

To address these questions concerning the dechlorination of PCE by PceA, molecular dynamics (MD) simulations and quantum mechanical/molecular mechanical (QM/MM) calculations have been carried out. Our studies demonstrate that the most favored mechanism involves an

inner-sphere C-Cl homolysis followed by PCET. In particular, our calculations reveal that the proximal [4Fe-4S]$^{1+}$ cluster participates as an electron donor, mediating a PCET process that quenches the radical intermediate. Thus, the proximal [4Fe-4S]$^{1+}$ cluster is non-innocent in the PceA catalysis. Moreover, our study demonstrates that the efficient proton donor is Arg305, which has not been anticipated previously.[13,29,30]

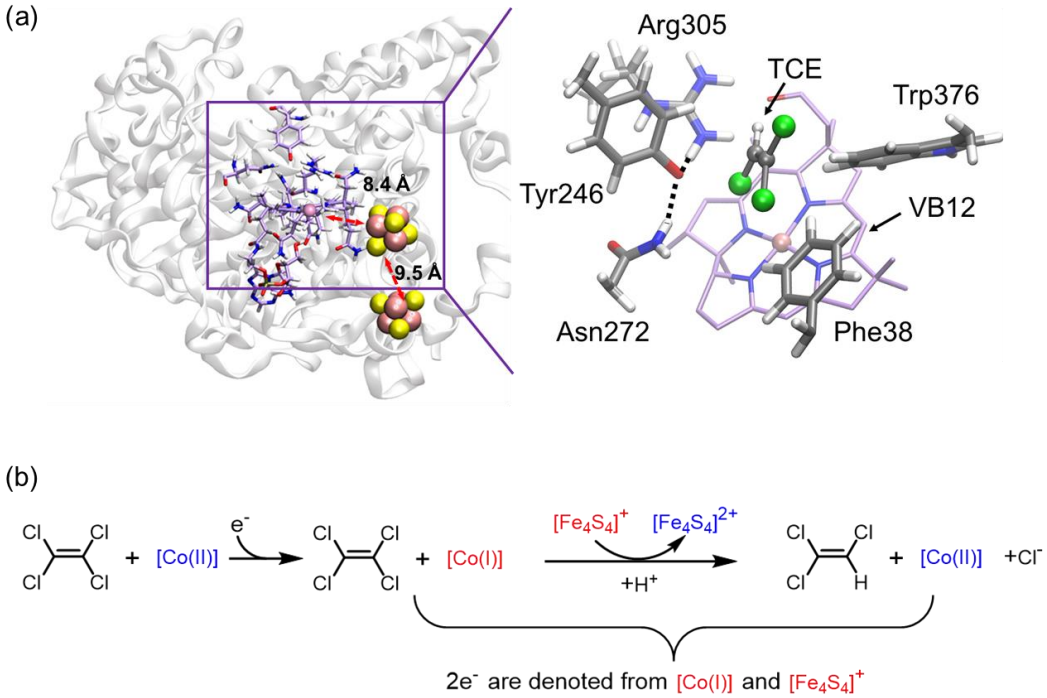

Figure 1. Structure and mechanism of PceA. (a) Crystal structure of PceA in complex with TCE (PDB: 4URo). Distances between the closest Fe atoms of the [4Fe-4S] clusters and the Co atom of the norpseudo-B12 are shown in red arrows. (b) Overall reactions for the reductive dechlorination of PCE catalyzed by PceA.

2.METHODS

2.1 System setup and MD simulation. The crystal structure of the PceA complexed with the substrate TCE (PDB:4URo) was used to build the model system. The TCE molecule was manually replaced with PCE. Only chain B was retained in our study. The protonation states of titratable residues (His, Glu, Asp) were assigned on the basis of pK_a values by PROPKA[31] and visual inspection of local H-bonding networks. Histidine residues His40, His357 and His449 were protonated at the δ position, His187 and His400 were protonated at the ε position, and the glutamic acid residue Glu33 whose pK_a value is 8.24, was protonated. All other Asp and Glu residues were deprotonated. Because the protonation state of Tyr246 has been debated with reference to the crystal structure[13] and in previous computational studies,[29,30] both the protonated and deprotonated states of Tyr246 were considered in our study. The LEAP module in Amber 18[32] was used to add the missing hydrogen atoms. The general AMBER force field (GAFF[33]) was used for the substrate, PCE, while the RESP method[34] was used to calculate the partial atomic charges at HF/6-31G*. The force field for the cobalamin active site and the [4Fe-4S] cluster were parameterized using the MCPB.[35] To neutralize the total charge of the system, 10 Na^+ ions were added to the surface of the protein, and the resulting protein was solvated with a 15 Å layer of TIP3P[36] waters. We used the Amber ff14SB[37] force field for the protein residues.

After the setup, the energy of the system was minimized by 5000 steps of steepest descent and 5000 steps of conjugate gradient methods. Then the system was heated from 0 K to 300 K under a canonical ensemble for 0.5 ns with a 2 fs time step. Subsequently, a 1 ns density equilibration was performed under the NPT ensemble at 300 K and 1.0 atm pressure to get a uniform density after the heating dynamics. Subsequently, we removed all restraints on the protein and further equilibrated the system for 4 ns under an NPT ensemble to obtain the well settled pressure and temperature. Finally, a productive MD run was conducted for 50 ns. During all MD simulations, the covalent bonds containing hydrogen were constrained using SHAKE.[38] All simulations were performed with the GPU version of the Amber 18 package.[32]

2.2 QM/MM methodology. All QM/MM calculations were performed using ChemShell,[39] combining Turbomole[40] for the QM region and DL_POLY[41] for the MM region. Residues within 12.0 Å of the Co atom were included into the active region. The electronic embedding[42] scheme was employed to account for the polarizing effect of the enzyme environment on the QM region. Hydrogen link atoms[43] with the charge-shift model[44] were applied to treat the QM/MM boundary. B3LYP[45] has been proved to be a successful functional for studying iron-based metalloenzymes[46] and cobalamin systems in previous studies.[29,47] During QM/MM calculations, the QM region was studied by B3LYP at two levels of theory. The QM region consists of the truncated cobalamin, the proximal [4Fe-4S] cluster,

the PCE substrate, the side chains of Tyr382, Tyr246, Arg305, Glu33, and several key water molecules (see Figure S1). For geometry optimization, all-electron basis of Def2-SVP (labeled B1) was used. The energies were further corrected with the larger basis set Def2-TZVP (labeled B2). The dispersion correction was included with Grimme's D3BJ[48] method. The DL-FIND[49] optimizer was used in the geometry optimization. The transition states were determined as the highest point on the potential energy surface along the reaction coordinates, for which a small increment of 0.02 Å was used for scanning near the transition states. All transition states (TSs) were located by relaxed potential energy surface (PES) scans followed by the full TS optimizations using the P-RFO optimizer. Given the high computational cost of QM/MM MD-based free energy calculations and the very large QM region (148 atoms) in the present study, we use the electronic energy barriers as estimates of the free energy barriers in the enzyme. For comparison, we also tested the first step of mechanism (ii) (inner-sphere C-Cl homolysis process) with QM/MM MD-based metadynamics, which gives a free energy barrier of 4.4 kcal/mol (Figure S20). Such free energy barrier of 4.4 kcal/mol is in close agreement with the electronic energy barrier of 3.4 kcal/mol (Figure 4), suggesting that the entropy correction plays minor effects in the catalytic reactions of metalloenzymes.[50-52]

2.3 Electronic structure of the [4Fe-4S]$^{1+}$ cluster in PceA. In cases in which the [4Fe-4S]$^{1+}$ cluster acts as the electron donor in the dehalogenation in PceA, six broken-symmetry electronic states of [4Fe-4S]$^{1+}$ cluster were considered[53-56] (See Figure S2). In the [4Fe-4S]$^{1+}$ cluster, the exchange interactions of d-electrons favors the high-spin state on each individual Fe, while super-exchange interactions between different Fe atoms favor the antiferromagnetic coupling between the Fe-Fe pairs.[57,58] Thus, the [4Fe-4S] cluster normally has a low-spin ground state, e.g. S=1/2 for [4Fe-4S]$^{1+}$.[59] According to the spin-coupling combinations of four Fe atoms, six electronic states are available for the [4Fe-4S] cluster (Figure S2). For instance, as shown in Scheme 1, ααββ denotes that Fe1 and Fe2 have the net spin of α, while Fe3 and Fe4 have the net spin of β.

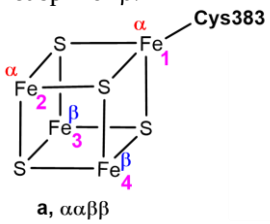

Scheme 1. Illustration of one of the six electron states of [4Fe-4S] cluster considered in this study, a: ααββ. α and β represent the orientation of 3d orbital electrons on each Fe. (The b-f states are shown in Figure S2)

The low-lying electronic states of [4Fe-4S] cluster are complicated and single-reference DFT calculations may not perfectly describe all the low-lying electronic states.[60] However, only the ground states of the [4Fe-4S]$^{+}$ and [4Fe-4S]$^{2+}$ species are involved in the present study, and the singlet ground state wavefunction of the [4Fe-4S] cluster from the broken-symmetry DFT (BS-DFT)[61] has the same spin coupling pattern with that from DMRG-CASSCF[60]. In addition, BS-DFT has been proven to be practical for studying catalytic reactions of metalloenzymes.[56,62-71] For example, a recent work has shown that BS-DFT methods are reliable for the electronic structure of FeMoco in nitrogenase,[72] as well as for redox potential calculations in iron-sulfur clusters.[73] Unlike small model [4Fe-4S] clusters,[60,74-76] the current system with a large QM region (148 atoms) is challenging to study with MC-SCF methods. As such, we think that BS-DFT is still a practical method for studying catalytic reactions in complex metalloenzymes like PceA, despite its well-known deficiencies.

3.RESULTS AND DISCUSSION

3.1 Possible mechanisms of dechlorination investigated in this study. As shown in Figure 1a, the binding conformation of the substrate is unfavorable for the nucleophilic attack of Co(I) on the carbon of PCE. This disfavors mechanisms where [Co(III)]-C species is the intermediate proposed based on in vitro cobalamin dechlorination studies.[77,78] This is in line with our QM/MM calculations, showing that nucleophilic attack of Co(I) onto PCE requires a high activation energy, over 55 kcal/mol (see Figure S8). Thus, mechanisms involving the formation of Co-C bond can be ruled out safely.

Since both the Co(I) and the proximal [4Fe-4S]$^{1+}$ cluster may function as electron donors for PceA reactions, we consider the four electron-transfer routes, (I)-(IV), which are displayed in Scheme 2.

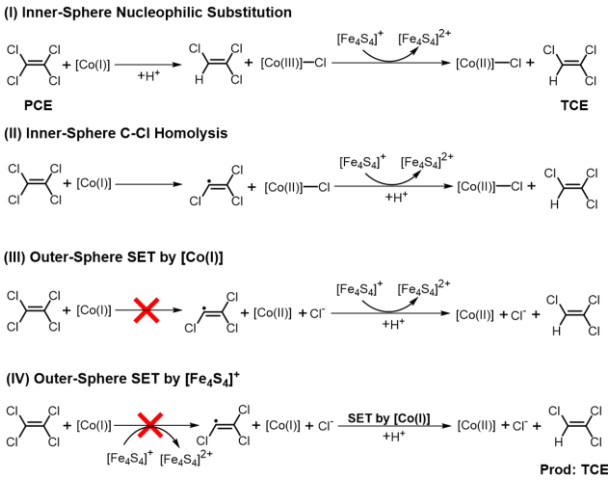

Scheme 2. Mechanisms proposed in the present work for dechlorination of PCE by PceA.

Mechanisms (I) and (II) contain the formation of Co-Cl bond. In mechanism (I), the nucleophilic attack by [Co(I)] on a Cl substituent of PCE is coupled with the proton transfer to the substrate, leading to the formation of TCE and [Co(III)]-Cl. In mechanism (II), a Co(I) mediated C-Cl bond homolysis firstly produces the substrate radical, which is followed by a [4Fe-4S]$^{1+}$-mediated PCET to quench the radical, affording the product.

Mechanisms (III) and (IV) involve an outer-sphere single electron transfer (SET) mechanism mediated by either the Co(I) center or the [4Fe-4S]$^{1+}$. However, our QM/MM calculations show that the reductive C-Cl cleavage *via* either one of the outer-sphere mechanisms (III) and (IV) are highly unfavorable thermodynamically. For mechanism (III), our QM/MM-scanning shows that the energy in-

creases steadily as the C-Cl distance increases, and no stable intermediate can be located along the scanned energy profile (Figure S9). In mechanism (IV), the C-Cl elongation first causes a conformational change of the substrate, and further C-Cl elongation leads to the steady increase in energy (Figure S10). Thus, both mechanisms (III) and (IV) can be reasonably ruled out.

Therefore, in the following sections, we focus on mechanisms (I) and (II) in Scheme 2. In particular, both the Tyr246-deprotonated and Tyr246-protonated states will be discussed and compared.

3.2 Source of the proton. Dechlorination requires proton to complete the catalytic transformation (Scheme 2). However, the proton source has been highly controversial.[13,29,30] Since the absolute pK_a is relatively challenging to compute, we have estimated the pK_a shift in the presence of Arg305 and Asn272. Our calculations suggest the presence of H-bonding interactions from Arg305 and Asn272 can reduce the pK_a of Ty246 by ~3.7 (Figure S21). Such value is roughly consistent with what has been found in acetoacetate decarboxylase.[79] As the normal tyrosine has a pK_a value of 10.1, the pK_a with Arg305 and Asn272 is estimated to be 10.1-3.7=6.4. Such pK_a value of 6.4 suggests that Tyr246 is in the deprotonated state in the experimental pH (7.5~8).[13] Thus, the low pK_a of Tyr246 is caused by the two strong H-bonds with Asn272 and the positively charged Arg305. To elucidate the source of the proton, we performed two different MD simulations on PceA in complex with PCE: one uses a protonated Tyr246 residue and the other a deprotonated Tyr246. Figure 2 shows representative snapshots from these MD simulations. Different from the crystal structure (PDB: 4UR0) where the substrate is slightly far away from the Co atom as a water molecule is axially coordinated to the Co atom. Both MD simulations on Tyr246-protonated and Tyr246-deprotonated states show that the water molecule was spontaneously dissociated from Co(I) and thus the substrate can approach the Co atom as shown in Figure 2. Such finding suggests that the Co(I) center has quite weak binding affinity for water.

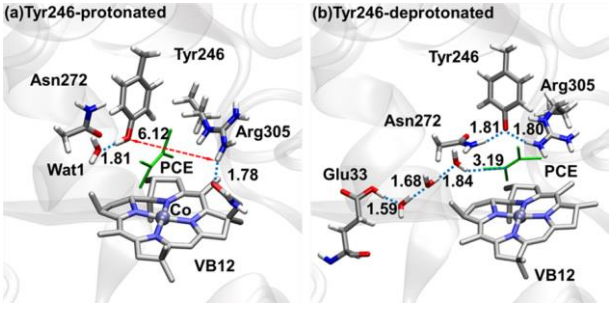

Figure 2. Representative snapshots during the MD simulations of protonated and deprotonated Tyr246 states in PceA. (a) The active site and H-bonding networks for the Tyr246-protonated state; (b) The active site and H-bonding networks for the Tyr246-deprotonated state. Key distances are given in Å.

When Tyr246 is protonated, the two H-bonds with Asn272 and Arg305 which exist in the crystal structure (shown in Figure 1a) are completely broken (see Figure 2a). Instead, the hydroxyl group of Tyr246 forms a new H-bond with a neighboring water molecule (Figure 2a), while Arg305 forms a strong H-bond with the amide group from the corrin ring. However, when Tyr246 is deprotonated, (Figure 2b), Asn272 and Arg305 form two strong H-bonds with the O atom of Tyr246, with O-H distances of 1.81Å and 1.80Å, respectively. Such H-bonding networks are in good agreement with the crystal structure,[13] *indicating that Tyr246 should be deprotonated.*

For the Tyr246-deprotonated state (Fig. 2b), no proton channel is available for the protonation of the Tyr246-O$^-$. In addition, the negatively charged Tyr246-O$^-$ forms two strong H-bonds with Arg305 and Asn272, which inhibits the protonation of Tyr246-O$^-$. Given these two factors, the deprotonated Tyr246 could not possibly function as the proton donor for the catalysis of PceA. Indeed, we have investigated the mechanism (I) and (II) with the protonated Tyr246, and found the reactions are quite unfavorable compared to the one reported later in Figure 5 (the detailed results and discussions can be found in Figure S3-S7 and relevant discussions in SI). For the deprotonated Tyr246 state, there are two possible proton sources: (1) the active site residue Arg305, which is in proximity to PCE, may function as a proton donor for the catalysis, and (2) the protonated Glu33 which form a water chain to PCE and, may constitute another proton source. Both two proton sources have been considered later.

3.3 Mechanism (I) with the deprotonated Tyr246 (Fig. 2b). For mechanism (I), the reaction is initiated by the nucleophilic attack of [Co(I)] on the chloride, which is coupled with the proton transfer to the substrate (see Scheme 2). In cases in which Tyr246 is deprotonated, both Arg305 and the protonated Glu33 can be the possible proton source (see Figure 2b). For mechanism (I) with the proton source of Arg305, our QM/MM calculations show the reaction has a barrier of 20.1 kcal/mol, leading to the product TCE in a single step (Figure 3 and Figure S11). If the protonated Glu33 acts as the proton donor, the reaction requires a slightly higher barrier of 21.3 kcal/mol (Figure S12), indicating that Arg305 is slightly favored over the protonated Glu33 in the proton donation for mechanism (I).

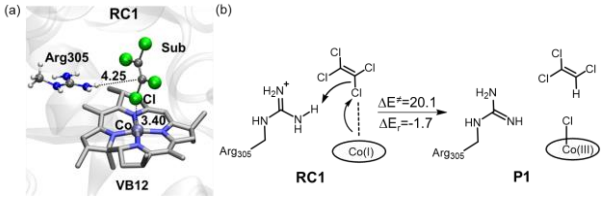

Figure 3. QM/MM calculated results for the first step reaction in the dechlorination of PCE through mechanism (I) in the Tyr246-deprotonated state (Arg305 acting as the proton source). (a) QM(UB3LYP/B1)/MM-optimized reactant RC1. (b) QM(UB3LYP/B2)/MM-calculated barrier (kcal/mol) in this step. The dispersion corrections are included in the relative energies. Key distances are given in Å

3.4 Mechanism (II) with the deprotonated Tyr246 (Fig. 2b). In mechanism (II), in Scheme 2, the first step involves a reductive cleavage of the C-Cl bond, leading to [Co(II)]-Cl species and a substrate radical species. As shown in Figure 4, starting from RC2 (same structure as RC1, is denoted here as RC2), Co(I) can donate an electron to facilitate the homolytic C-Cl bond cleavage, while the departing Cl^- ion can coordinate simultaneously to Co, forming [Co(II)-Cl] species. This step has a tiny barrier of 3.4 kcal/mol, which is quite favorable kinetically (also see Figure S13).

In the second step of mechanism (II), the $[4Fe\text{-}4S]^{1+}$ cluster functions as an electron donor to mediate a plausible PCET process, that quenches the TCE radical, and produces TCE (Scheme 2 (II)). In this process, the proton can be supplied by the Arg305 or the protonated Glu33 (see Figure 2b).

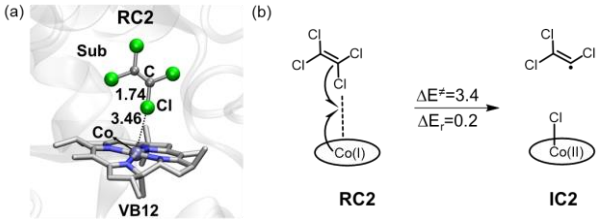

Figure 4. QM/MM calculated results for the first step reaction in the dechlorination of PCE through mechanism (II) in the Tyr246-deprotonated state. (a) QM(UB3LYP/B1)/MM-optimized reactant RC2. (b) QM(UB3LYP/B2)/MM-calculated barrier (kcal/mol) in this step. The dispersion corrections are included in the relative energies. Key distances are given in Å.

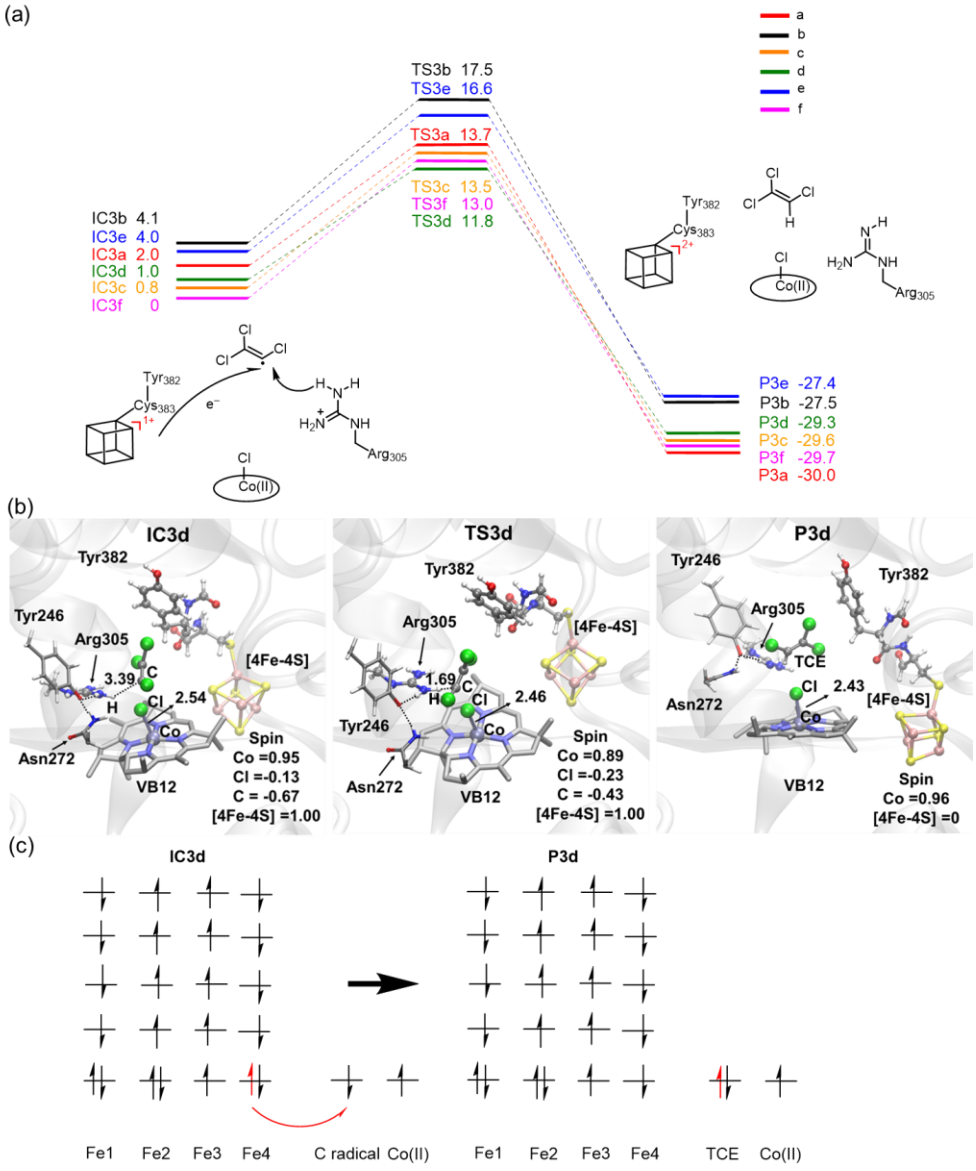

Figure 5. QM/MM calculated results for the second step reaction in the dechlorination of PCE through mechanism (II) in the Tyr246-deprotonated state. (a) QM(UB3LYP/B2)/MM relative energies (kcal/mol) in six electronic states (a, αααβ; b, αβαβ; c, αββα; d, βααβ; e, βαβα; f, βββα), shown alongside the schematic drawings of species involved in the reaction pathways (Arg305 acting as the proton source). The dispersion corrections are included in the relative energies. (b) QM(UB3LYP/B1)/MM-optimized geometries of key species involved in the reaction. (c) The electron shift diagrams for [4Fe-4S]-mediated PCET reaction in mechanism (II). Key distances are given in Å

Figure 5a shows the QM/MM calculated energy profile for this PCET process (Arg305 acting as the proton source) in all six broken-symmetry electronic states,[54-56] while Figure 5b displays the QM/MM optimized structures involved in the most reactive electronic state (state d). As shown in Figure 5a, the six electronic states are almost degenerate energetically. The relative barriers of PCET can be largely correlated with the relative energies of different electronic states of IC3. In IC3d, it is seen that Arg305 maintains a short distance of 3.39Å to the carbon of PCE. Starting from IC3d, the proton transfer from the Arg305 to the carbon of PCE can drive the electron transfer from the $[4Fe\text{-}4S]^{1+}$ cluster to the substrate radical, leading to the formation of $[4Fe\text{-}4S]^{2+}$ cluster and the product, TCE.

As shown in Figure 5a, the lowest barrier via TS3d is moderate, 11.8 kcal/mol, and the reaction exothermicity is ~30 kcal/mol, indicating this PCET process is quite favorable kinetically and thermodynamically. For comparison, we also investigated the alternative proton source of the protonated Glu33 (Figure S14). However, at the most reactive electronic state, the Glu33-mediated PCET has a higher barrier of 16.5 kcal/mol, indicating *the Arg305-mediated PCET process is favored over that of the Glu33-mediated pathway*.

Inspection of Figure 5b shows that the distance between the substrate C atom and the H atom of Arg305 has decreased from 3.39 Å in IC3d to 1.69 Å in TS3d. However, the spin population of the $[4Fe\text{-}4S]^{1+}$ cluster remains the same in IC3d and TS3d (Figure 5b). All these observations suggest that the proton transfer precedes the electron transfer. After surmounting TS3d, one electron from $[4Fe\text{-}4S]^{1+}$ is spontaneously transferred to the substrate, and thereby facilitates the subsequent proton transfer to the substrate, and generating the final TCE product. Clearly, the proton transfer from Arg305 to the substrate radical triggers the electron transfer from $[4Fe\text{-}4S]^{1+}$ to the substrate radical, leading to an asynchronous PCET.

Figure 5c shows the electron shift diagrams for the representative electronic state (IC3d→P3d), while other electronic states share similar electron shift diagrams. In all the six electronic states, the $[4Fe\text{-}4S]^{1+}$ cluster can supply a spin-up α electron rather than a β electron for the PCET reaction (see Figure 5c). Upon the donation of an α electron, the d-block of Fe4 achieves five spin-parallel electrons (right panel, Figure 5c), which brings about *the maximum exchange stabilization*[80-82] in the Fe4 block. In addition, all d-electrons in the right-hand $[4Fe\text{-}4S]^{2+}$ cluster are now antiferromagnetically coupled (9 α electrons *vs.* 9 β electrons), and this leads to a *maximum super-exchange interactions* in the $[4Fe\text{-}4S]^{2+}$ cluster.[83] Thus, the electron transfer during the PCET process is enhanced by both exchange and super-exchange stabilizing interactions.[65]

Once the product TCE was generated in P3d, we assume it would diffuse out of the active site, as evidenced from experiments.[23] As Arg305 is deprotonated after PCET (see Figure 5), it has to be re-protonated for the next cycle. To identify the plausible proton channel, we have carried out MD simulations, which revealed an obvious proton channel consisting of the protonated Glu33 and six water molecules (Figure S22).

3.5 The Tyr246-deprotonated state has evolved to accelerate the catalysis of PceA. Among all the mechanisms that have been investigated, our study demonstrates that the stepwise inner-sphere mechanism (II), which is mediated by the $[4Fe\text{-}4S]^{1+}$ cluster and Arg305 in the Tyr246-deprotonated state, is the most favorable pathway for the PceA-catalyzed dechlorination of PCE.

In the Tyr246-protonated state, our MD simulations show that the original H-bonding interactions with Arg305 and Asn272 is completely disrupted (Figure 2a). This leaves Tyr246 as the only feasible proton donor for the PCET reaction, which occurs at the expense of a high barrier of 21.3 kcal/mol (Figure S5 and S6), ~10 kcal/mol higher than the Arg305-mediated PCET process in the Tyr246-deprotonated state (TS3d in Figure 5). Obviously, the deprotonation of Tyr246 remarkably accelerates the catalysis of PceA. Such a finding may well rationalize the catalytic roles of highly conserved Tyr246, Asn272 and Arg305. On one hand, the strong H-bonding interactions with both Asn272 and Arg305 can maintain the deprotonated state for Tyr246, which can in turn stabilize the conformation of Arg305 for proton donation (Figure 2b). By contrast, with a protonated Tyr246, Arg305 will undergo fast conformational change and move away from the substrate (Figure 2a).

Moreover, the weak salt-bridge interaction between Tyr-O^- and Arg305 is favorable for the proton donation by Arg305, which can in turn facilitate the PCET reaction. To verify this hypothesis, we compared the acidity of Arg305 with the salt-bridge interaction of Tyr-O^- against that of a carboxylic acid, while the salt-bridge interaction with Glu/Asp residues is strong and quite prevalent in proteins. Our QM model calculations show that the deprotonation energy of Arg305 with a carboxylic acid is 4.71 kcal/mol higher than that of Arg305 with Try-O^- (Figure S15). Obviously, the Tyr246-deprotonated state is favorable for the proton donation from Arg305, which can in turn facilitate the PCET reaction.

3.6 Further validation of our mechanism. In the EPR experiment by Diekert et. al, the lack of a $^{35}Cl/^{37}Cl$ (super)hyperfine splitting (denoted as A_{II}) leads them to rule out the existence of [Co(II)]-Cl species in PceA-PCE.[23] However, in the presence of excess chloride salts, Leys and coworkers measured an $A_{II}(^{35}Cl)$ value of ~70 MHz for the [Co(II)]-Cl species in NpRdhA, which is an another B12-dependent RDase.[14] For comparison, we also calculated the $A_{II}(^{35}Cl)$ value of the [Co(II)]-Cl species on the basis of a cluster model of PceA by ORCA (Figure S16).[84-87] Our calculations led to an $A_{II}(^{35}Cl)$ value of 58 MHz, which is close to the value determined by EPR experiment. Thus, both EPR experiments and our calculations indicates that the $A_{II}(^{35}Cl)$ value of [Co(II)]-Cl species is rather small, suggesting that detection of [Co(II)]-Cl species during the catalytic cycle requires EPR experiments with high resolution. In addition, if the chloride ion undergone a fast dissociation from the [Co(II)]-Cl species during the catalytic cycle,

the short-lived [Co(II)]-Cl species could avoid any spectroscopy detection. To verify such possibility, we have investigated the Cl^- dissociation with and without a single electron transfer from $[4Fe\text{-}4S]^{1+}$ cluster. Our calculations show the direct Cl^- dissociation without the participation of an electron is unfavorable kinetically and thermodynamically (Figure S17). However, when a SET from $[4Fe\text{-}4S]^{1+}$ cluster is involved, the Cl^- dissociation will occur spontaneously. In addition, our calculations show that such SET process is quite favorable thermodynamically, with an exothermicity of 9.3 kcal/mol (Figure S18).

In a very recent study, Brunold and coworkers proposed the Co(I)-mediated SET mechanism (see mechanism (III) shown in Scheme 2) using the ONIOM calculations.[30] In this study, the leaving chloride ion can be stabilized by the Arg305 and the amide group of the B12 cofactor. To verify this possibility, we have constructed a similar structure according to this work. However, our QM/MM optimization shows that the Cl^- dissociated intermediate is unstable, and gets ultimately coordinated to Co(II) (Figure S19). Along with our finding that Co(I)-mediated SET mechanism is highly unfavorable kinetically and thermodynamically (Figure S9), we assume that the Co(I)-mediated SET mechanism is unlikely for chloroalkenes. Given that C-Br bond is much weaker and a better electron acceptor than C-Cl bond, we expect that Co(I)-mediated SET mechanism would be more accessible for the degradation of bromoalkenes, especially for the aromatic bromide with low reduction potential. Such substrate-dependent reactivity of RDases is worthwhile to investigate in our future work.

3.7 Catalytic cycle of the PCE dechlorination by PceA. Based on our comprehensive computational study, we propose a catalytic cycle of PceA in Scheme 3. Starting from the reduced Co(I) state (1), the Co(I) mediated C-Cl bond homolysis firstly affords the [Co(II)]-Cl species and the substrate radical (2). Such reaction step was demonstrated to be facile in our QM/MM study and previous study.[29] Then, our calculations reveal that the radical quenching is mediated by an unusual PCET process, during which the proton is donated by the adjacent Arg305 residue, while the electron is donated by the proximal $[4Fe\text{-}4S]^{1+}$ cluster. Such reaction step affords the product TCE, along with the [Co(II)]-Cl intermediate (3). Though the function of $[4Fe\text{-}4S]^{1+}$ cluster as the electron donor in reducing Co(II) is well recognized in RDases, its participation in mediating a PCET process is unexpected in previous experimental and computational studies. Given that in some reductive dehalogenases (e.g. NpRdhA[14]), the position of Arg is replaced by a Lys residue, it is possible that Lys residue may serve similar roles as Arg. Such possibility warrants examination in further study. Our study suggests that the final dissociation of Cl^- can be assisted by a SET from $[4Fe\text{-}4S]^{1+}$ cluster, which would lead to the formation of [Co(I)] for the next cycle.

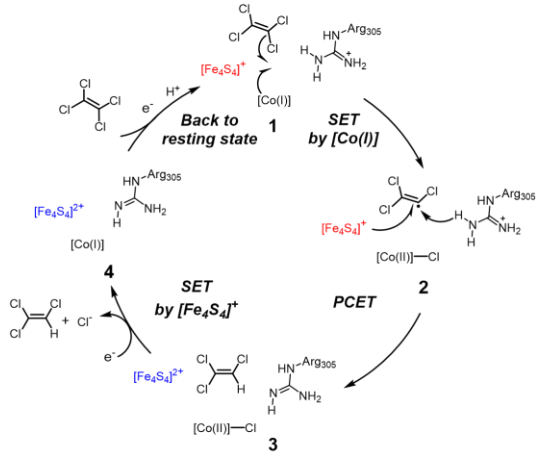

Scheme 3. Catalytic cycle of the PCE dechlorination by PceA.

3.8 Radical quenching via the PCET reaction in [4Fe-4S]-dependent metalloenzymes. [4Fe-4S]-dependent metalloenzymes are widespread in organisms.[88-90] In addition to [4Fe-4S]-dependent reductive dehalogenases, a superfamily includes the [4Fe-4S]-dependent radical S-adenosylmethionine (SAM) proteins, which can

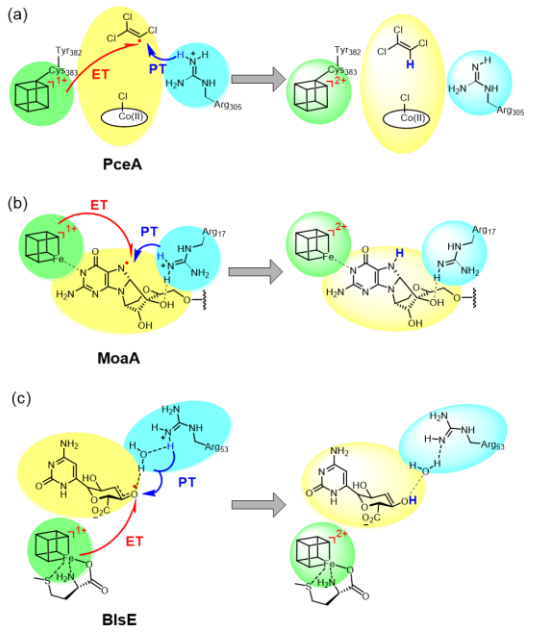

Figure 6. PCET-mediated radical quenching in [4Fe-4S]-dependent metalloenzymes: (a) the cobalamin(B12)-dependent enzyme PceA; (b) the radical SAM enzyme MoaA; (c) the radical SAM enzyme BlsE.

catalyze a panoply of challenging transformations using the common 5'-dAdo radical intermediate.[91-95] In the cobalamin(B12)-dependent PceA dechlorination on PCE, we have shown that an unexpected PCET reaction is involved in the radical quenching, during which the electron is donated by the proximal [4Fe-4S] cluster, and the proton comes from the adjacent Arg305 residue (see Figure 6a). Interestingly, this finding is reminiscent of the radical SAM enzyme MoaA,[63] in which a PCET process mediated by the adjacent Arg17 residue and the auxiliary [4Fe-4S] cluster have been proposed for the reduction of the N-centered

radical intermediates in the catalytic cycle (see Figure 6b). We expect that a similar PCET process could be participated to quench an enol radical intermediate in the radical SAM enzyme BlsE,[64] producing the enol intermediate (see Figure 6c). Thus, the radical quenching by the [4Fe-4S]$^{1+}$-mediated PCET could be a common mechanism in [4Fe-4S]-dependent metalloenzymes.

3.9 Dechlorination of TCE by PceA. We also investigated the dechlorination of TCE by PceA, which affords the product of *cis*-1.2-DCE.[13] As our study shows that mechanism (II), which involved an inner-sphere C-Cl homolysis followed by [4Fe-4S]$^{1+}$-mediated PCET is greatly favored over other three mechanisms for PCE, all our QM/MM calculations of TCE are limited to mechanism (II). On the basis of crystal structure of PceA-TCE complex (PDB:4URo), MD simulations (Figure S25 and S26) have been performed. As shown in Figure 7 and Figure S25, three representative conformations (A, B, C) were characterized from clustering analysis, while the ratio of A, B and C are 61.1%, 1.2% and 37.6% respectively. As shown in Figure 7a, for the major conformation A, our QM/MM calculations show that the first step for the reductive cleavage of the C-Cl bond involves a barrier of 8.1 kcal/mol and endothermicity of 4.9 kcal/mol relative to RC8 (Figure S27). For the second step of Arg305 and [4Fe-4S]$^{1+}$-mediated PCET process, the reaction involves a barrier of 11.5 kcal/mol at the most reactive electronic state (d, βααβ) (Figure S28). Thus, the dechlorination reaction has an overall barrier of 4.9+11.5=16.4 kcal/mol and the product for the conformation A is *cis*-1,2-DCE. Similarly, the QM/MM calculated barriers are 7.4+11.2=18.6 kcal/mol in conformation B (Figure S7b and Figure S29-S30) and 9.8+11.4=21.2 kcal/mol in conformation C (Figure 7c and Figure S31-S32), respectively. Given that the population of conformation A (61.1%) is much higher than that of conformation B (1.2%) and the barrier of dechlorination in conformation A ($\Delta E^{\neq}$=16.4 kcal/mol) is lower than that in conformation B ($\Delta E^{\neq}$=18.6 kcal/mol), the reaction would lead to the major product of *cis*-1,2-DCE, which is in good agreement with the experimental finding.[13]

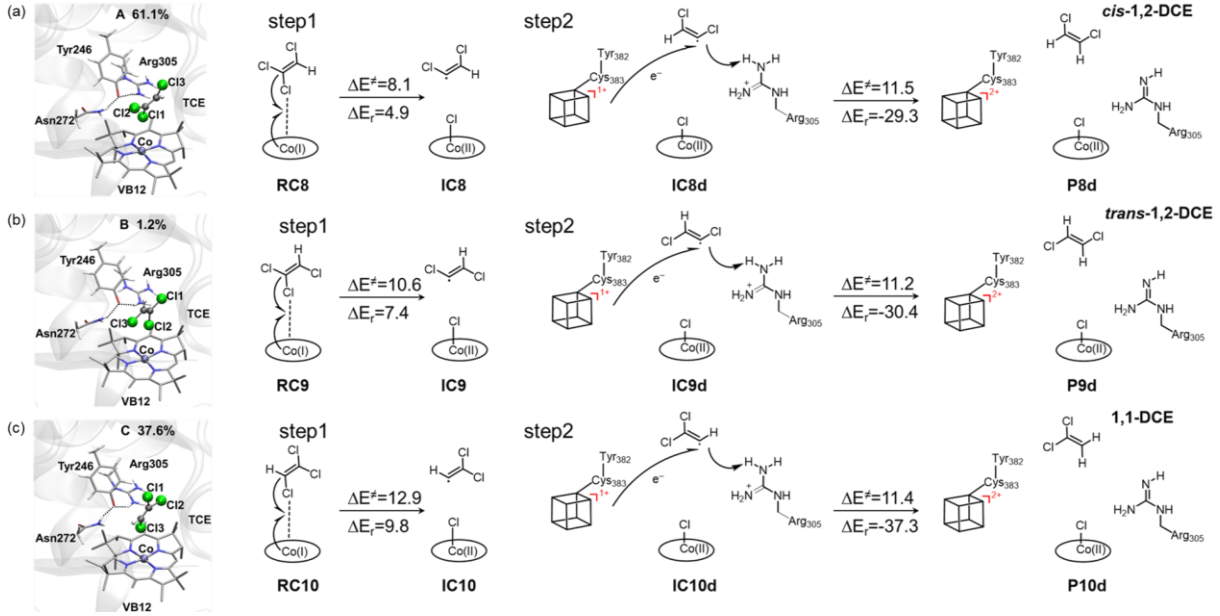

Figure 7. Three representative conformations (A, B, C) of TCE characterized from clustering analysis of MD simulations and QM(UB3LYP/B2)/MM-calculated barriers (kcal/mol) for the dechlorination of TCE through mechanism (II) in the Tyr246-deprotonated state. The dispersion corrections are included in the relative energies. (a) Conformation A. (b) Conformation B and (c) Conformation C.

4. CONCLUSION

In this study, we have performed MD simulations and QM/MM calculations to investigate the molecular mechanism of the dechlorination of PCE and TCE by reductive dehalogenase PceA. Among various mechanisms (I to IV, shown in Scheme 2) investigated in this study, we found that mechanism II, which involved an inner-sphere C-Cl homolysis followed by PCET is greatly favored over other three mechanisms.

Specifically, our calculations show that the proximal [4Fe-4S] cluster can mediate a PCET process to quench the TCE radical. Such the [4Fe-4S]-mediated *PCET process is enhanced by both exchange and super-exchange stabilizing interactions*. In this process, the proton is supplied by the active site residue Arg305 rather than by the widely-proposed Tyr246. The deprotonated state of Tyr246 is maintained by the H-bonding interactions with Asn272 and Arg305, and is critical to the dechlorination of PCE. The Tyr246-deprotonated state not only serves to maintain the favorable conformation of Arg305 for catalysis, but also sustains the proton donation ability of Arg305, whereas the acidity of Arg305 is key to the rate-determining PCET reaction. Though the function of [4Fe-4S]$^{1+}$ cluster as the electron donor in reducing Co(II) is well recognized in RDases, its participation in mediating a PCET process is unexpected in previous experimental and computational studies. Such [4Fe-4S]$^{1+}$-mediated PCET could be a common mechanism for radical quench in [4Fe-4S]-dependent

metalloenzymes. Given that different haloalkene substrate have different C-X bond strength (X=halogen), different polarizability of the dissociated X^-, as well as the different redox potential, we expect that RDases may adopt flexible routes for the degradation of various haloalkenes.

ASSOCIATED CONTENT

Supporting Information.
QM/MM results, calculated spin densities, QM/MM energies, the cartesian coordinates of all computed species. The material is available free of charge via the Internet at http://pubs.acs.org.

AUTHOR INFORMATION

Corresponding Author

*sason@yfaat.ch.huji.ac.il
*wangbinju2018@xmu.edu.cn

Author Contributions

ORCID

Sason Shaik: 0000-0001-7643-9421
Binju Wang: 0000-0002-3353-9411

Notes

The authors declare no competing financial interest.

ACKNOWLEDGMENT

This work was supported by NSFC (No.22122305, 21907082 and 22073077 to B. W.). S.S is supported by the ISF (grant No. 520/18).

ABBREVIATIONS

RDases, Reductive dehalogenases; PCE, perchloroethylene; TCE, trichloroethene; DCE, dichloroethylene; MD, molecular dynamics; QM/MM, quantum mechanical/molecular mechanical; SET, single electron transfer; PCET, proton-coupled electron transfer; ET, electron transfer; PT, proton transfer; SAM, S-adenosylmethionine.

REFERENCES

1 Stringer, R. L.; Johnston, P. A., Chlorine and the environment: An overview of the chlorine industry. *Environ. Sci. Pollut. R* **2001** 8, 146.
2 Newman, J.; Peat, T. S.; Richard, R.; Kan, L.; Swanson, P. E.; Affholter, J. A.; Holmes, I. H.; Schindler, J. F.; Unkefer, C. J.; Terwilliger, T. C., Haloalkane dehalogenases: Structure of a rhodococcus enzyme. *Biochemistry* **1999** 38, 16105-16114.
3 Lau, E. Y.; Kahn, K.; Bash, P. A.; Bruice, T. C., The importance of reactant positioning in enzyme catalysis: A hybrid quantum mechanics/molecular mechanics study of a haloalkane dehalogenase. *Proc. Natl. Acad. Sci. U. S. A.* **2000** 97, 9937-9942.
4 Pimviriyakul, P.; Chaiyen, P., Flavin-dependent dehalogenases. *Enzymes* **2020** 47, 365-397.
5 Wang, Y.; Liu, A., Carbon-fluorine bond cleavage mediated by metalloenzymes. *Chem. Soc. Rev.* **2020** 49, 4906-4925.
6 Wang, Y.; Davis, I.; Shin, I.; Xu, H.; Liu, A., Molecular rationale for partitioning between C–H and C–F bond activation in Heme-Dependent tyrosine hydroxylase. *J. Am. Chem. Soc.* **2021** 143, 4680-4693.
7 Jugder, B.-E.; Ertan, H.; Lee, M.; Manefield, M.; Marquis, C. P., Reductive dehalogenases come of age in biological destruction of organohalides. *Trends Biotechnol.* **2015** 33, 595-610.
8 Jugder, B.-E.; Ertan, H.; Bohl, S.; Lee, M.; Marquis, C. P.; Manefield, M., Organohalide respiring bacteria and reductive dehalogenases: Key tools in organohalide bioremediation. *Front Microbiol* **2016** 7, 1-12.
9 Smidt, H.; De Vos, W. M., Anaerobic microbial dehalogenation. *Annu. Rev. Microbiol.* **2004** 58, 43-73.
10 Kräutler, B.; Fieber, W.; Ostermann, S.; Fasching, M.; Ongania, K.-H.; Gruber, K.; Kratky, C.; Mikl, C.; Siebert, A.; Diekert, G., The cofactor of tetrachloroethene reductive dehalogenase of *Dehalospirillum multivorans* is norpseudo-B_{12}, a new type of a natural corrinoid. *Helv. Chim. Acta* **2003** 86, 3698-3716.
11 Moser, C. C.; Keske, J. M.; Warncke, K.; Farid, R. S.; Dutton, P. L., Nature of biological electron-transfer. *Nature* **1992** 355, 796-802.
12 Gray, H. B.; Winkler, J. R., Long-range electron transfer. *Proc. Natl. Acad. Sci.* **2005** 102, 3534-3539.
13 Bommer, M.; Kunze, C.; Fesseler, J.; Schubert, T.; Diekert, G.; Dobbek, H., Structural basis for organohalide respiration. *Science* **2014** 346, 455-458.
14 Payne, K. A.; Quezada, C. P.; Fisher, K.; Dunstan, M. S.; Collins, F. A.; Sjuts, H.; Levy, C.; Hay, S.; Rigby, S. E.; Leys, D., Reductive dehalogenase structure suggests a mechanism for B12-dependent dehalogenation. *Nature* **2015** 517, 513-516.
15 Jugder, B. E.; Bohl, S.; Lebhar, H.; Healey, R. D.; Manefield, M.; Marquis, C. P.; Lee, M., A bacterial chloroform reductive dehalogenase: purification and biochemical characterization. *Microb Biotechnol* **2017** 10, 1640-1648.
16 Jugder, B.-E.; Payne, K. A. P.; Fisher, K.; Bohl, S.; Lebhar, H.; Manefield, M.; Lee, M.; Leys, D.; Marquis, C. P., Heterologous production and purification of a functional chloroform reductive dehalogenase. *ACS Chem. Biol.* **2018** 13, 548-552.
17 Tang, S.; Edwards, E. A., Identification of *Dehalobacter* reductive dehalogenases that catalyse dechlorination of chloroform, 1,1,1-trichloroethane and 1,1-dichloroethane. *Phil. Trans. R. Soc. B* **2013** 368, 1-10.
18 Tang, S.; Gong, Y.; Edwards, E. A., Semi-Automatic in silico gap closure enabled de novo assembly of two dehalobacter genomes from metagenomic data. *PLoS ONE* **2012** 7, e52038.
19 Parthasarathy, A.; Stich, T. A.; Lohner, S. T.; Lesnefsky, A.; Britt, R. D.; Spormann, A. M., Biochemical and EPR-Spectroscopic investigation into heterologously expressed vinyl chloride reductive dehalogenase (VcrA) from *Dehalococcoides mccartyi* Strain VS. *J. Am. Chem. Soc.* **2015** 137, 3525-3532.
20 McMurdie, P. J.; Behrens, S. F.; Müller, J. A.; Göke, J.; Ritalahti, K. M.; Wagner, R.; Goltsman, E.; Lapidus, A.; Holmes, S.; Löffler, F. E.; Spormann, A. M., Localized plasticity in the streamlined genomes of vinyl chloride respiring *Dehalococcoides*. *PLoS Genetics* **2009** 5, 1-10.
21 Wagner, A.; Segler, L.; Kleinsteuber, S.; Sawers, G.; Smidt, H.; Lechner, U., Regulation of reductive dehalogenase gene transcription in *Dehalococcoides mccartyi*. *Phil. Trans. R. Soc. B* **2013** 368, 1-10.
22 Kube, M.; Beck, A.; Zinder, S. H.; Kuhl, H.; Reinhardt, R.; Adrian, L., Genome sequence of the chlorinated compound–respiring bacterium *Dehalococcoides* species strain CBDB1. *Nat. Biotechnol.* **2005** 23, 1269-1273.
23 Kunze, C.; Bommer, M.; Hagen, W. R.; Uksa, M.; Dobbek, H.; Schubert, T.; Diekert, G., Cobamide-mediated enzymatic reductive dehalogenation via long-range electron transfer. *Nat. Comm.* **2017** 8, 15858-15868.
24 Maillard, J.; Schumacher, W.; Vazquez, F.; Regeard, C.; Hagen, W. R.; Holliger, C., Characterization of the corrinoid iron-sulfur protein tetrachloroethene reductive dehalogenase of *Dehalobacter restrictus*. *Appl. Environ. Microb.* **2003** 69, 4628-4638.
25 Sjuts, H.; Fisher, K.; Dunstan, M. S.; Rigby, S. E.; Leys, D., Heterologous expression, purification and cofactor reconstitution

of the reductive dehalogenase PceA from Dehalobacter restrictus. *Protein Expres. Purif* **2012** 85, 224-229.
26 Lai, Q.; Li, G.; Shao, Z., Genome sequence of *Nitratireductor pacificus* type strain pht-3B. *J. Bacteriol.* **2012** 194, 6958-6958.
27 Neumann, A.; Siebert, A.; Trescher, T.; Reinhardt, S.; Wohlfarth, G.; Diekert, G., Tetrachloroethene reductive dehalogenase of Dehalospirillum multivorans : substrate specificity of the native enzyme and its corrinoid cofactor. *Arch. Microbiol.* **2002** 177, 420-426.
28 Ye, L.; Schilhabel, A.; Bartram, S.; Boland, W.; Diekert, G., Reductive dehalogenation of brominated ethenes by *Sulfurospirillum multivorans* and *Desulfitobacterium hafniense* PCE-S. *Environ. Microbiol.* **2010** 12, 501-509.
29 Liao, R.-Z.; Chen, S.-L.; Siegbahn, P. E. M., Unraveling the mechanism and regioselectivity of the B12-dependent reductive dehalogenase PceA. *Chem. Eur. J.* **2016** 22, 12391-12399.
30 Greenhalgh, E. D.; Kunze, C.; Schubert, T.; Diekert, G.; Brunold, T. C., A spectroscopically validated computational investigation of viable reaction intermediates in the catalytic cycle of the reductive dehalogenase PceA. *Biochemistry* **2021** 60, 2022-2032.
31 Li, H.; Robertson, A. D.; Jensen, J. H., Very fast empirical prediction and rationalization of protein pK_a values. *Proteins* **2005** 61, 704-721.
32 Case, D. A. I. Y. B.-S., I. Y.; S.R. Brozell, S. R.; Cerutti, D. S.; Cheatham, T. E.; Cruzeiro, III, V. W. D.; Darden, T. A.; Duke, R. E.; Ghoreishi, D.; Gilson, M. K.; Gohlke, H.; Goetz, A. W.; Greene, D.; Harris, R.; Homeyer, N.; Izadi, S.; Kovalenko, A.; Kurtzman, T.; Lee, T. S.; LeGrand, S.; Li, P.; Lin, C.; Liu, J.; Luchko, T.; Luo, R.; Mermelstein, D.J.; Merz, K. M.; Miao, Y.; Monard, G.; Nguyen, C.; Nguyen, H.; Omelyan, I.; Onufriev, A.; Pan, F.; Qi, R.; Roe, D. R.; Roitberg, A.; Sagui, C.; Schott-Verdugo, S.; Shen, J.; Simmerling, C. L.; Smith, J.; Salomon-Ferrer, R.; Swails, J.; Walker, R. C.; Wang, J.; Wei, H.; Wolf, R. M.; Wu, X.; Xiao, L.; York D. M.; Kollman, P. A., AMBER 2018, University of California, San Francisco. **2018**.
33 Wang, J. M.; Wolf, R. M.; Caldwell, J. W.; Kollman, P. A.; Case, D. A., Development and testing of a general amber force field. *J. Comput. Chem.* **2004** 25, 1157-1174.
34 Bayly, C. I.; Cieplak, P.; Cornell, W. D.; Kollman, P. A., A well-behaved electrostatic potential based method using charge restraints for deriving atomic charges: the RESP model. *J. Phys. Chem.* **1993** 97, 10269-10280.
35 Li, P.; Merz, K. M., Jr., MCPB.py: A python based metal center parameter builder. *J. Chem. Inf. Model.* **2016** 56, 599-604.
36 Jorgensen, W. L.; Chandrasekhar, J.; Madura, J. D.; Impey, R. W.; Klein, M. L., Comparison of simple potential functions for simulating liquid water. *J. Chem. Phys.* **1983** 79, 926-935.
37 Maier, J. A.; Martinez, C.; Kasavajhala, K.; Wickstrom, L.; Hauser, K. E.; Simmerling, C., ff14SB: Improving the accuracy of protein side chain and backbone parameters from ff99SB. *J. Chem. Theory Comput.* **2015** 11, 3696-3713.
38 Ryckaert, J. P.; Ciccotti, G.; Berendsen, H. J. C., Numerical integration of the cartesian equations of motion of a system with constraints: molecular dynamics of n-alkanes. *J. Comput. Phys.* **1977** 23, 327-341.
39 Sherwood, P.; de Vries, A. H.; Guest, M. F.; Schreckenbach, G.; Catlow, C. R. A.; French, S. A.; Sokol, A. A.; Bromley, S. T.; Thiel, W.; Turner, A. J.; Billeter, S.; Terstegen, F.; Thiel, S.; Kendrick, J.; Rogers, S. C.; Casci, J.; Watson, M.; King, F.; Karlsen, E.; Sjøvoll, M.; Fahmi, A.; Schäfer, A.; Lennartz, C., QUASI: A general purpose implementation of the QM/MM approach and its application to problems in catalysis. *J. Mol. Struc. (THEOCHEM)* **2003** 632, 1-28.
40 Ahlrichs, R.; Bar, M.; Haser, M.; Horn, H.; Kolmel, C., Electronic structure calculations on workstation computers: The program system turbomole. *Chem. Phys. Lett.* **1989** 162, 165-169.
41 Smith, W.; Forester, T. R., DL_POLY_2.0: A general-purpose parallel molecular dynamics simulation package. *J. Mol. Graphics.* **1996** 14, 136-141.
42 Bakowies, D.; Thiel, W., Hybrid models for combined quantum mechanical and molecular mechanical approaches. *J. Phys. Chem.* **1996** 100, 10580-10594.
43 de Vries, A. H.; Sherwood, P.; Collins, S. J.; Rigby, A. M.; Rigutto, M.; Kramer, G. J., Zeolite structure and reactivity by combined quantum-chemical−classical calculations. *J. Phys. Chem. B* **1999** 103, 6133-6141.
44 Sherwood, P.; de Vries, A. H.; Collins, S. J.; Greatbanks, S. P.; Burton, N. A.; Vincent, M. A.; Hillier, I. H., Computer simulation of zeolite structure and reactivity using embedded cluster methods. *Faraday Discuss.* **1997** 106, 79-92.
45 Lee, C.; Yang, W.; Parr, R. G., Development of the Colle-Salvetti correlation-energy formula into a functional of the electron density. *Phys. Rev. B* **1988** 37, 785-789.
46 Altun, A.; Breidung, J.; Neese, F.; Thiel, W., Correlated *ab initio* and density functional studies on H_2 activation by FeO^+. *J. Chem. Theory Comput.* **2014** 10, 3807-3820.
47 Liao, R.-Z.; Chen, S.-L.; Siegbahn, P. E. M., Which oxidation state initiates dehalogenation in the B12-dependent enzyme NpRdhA: Co^{II}, Co^{I}, or Co^{0}? *ACS Catal.* **2015** 5, 7350-7358.
48 Grimme, S., Accurate description of van der Waals complexes by density functional theory including empirical corrections. *J. Comput. Chem.* **2004** 25, 1463-1473.
49 Kaestner, J.; Carr, J. M.; Keal, T. W.; Thiel, W.; Wander, A.; Sherwood, P., DL-FIND: An open-source geometry optimizer for atomistic simulations. *J. Phys. Chem. A* **2009** 113, 11856-11865.
50 Wang, B.; Cao, Z.; Sharon, D. A.; Shaik, S., Computations Reveal a Rich Mechanistic Variation of Demethylation of N-Methylated DNA/RNA Nucleotides by FTO. *ACS Catal.* **2015** 5, 7077-7090.
51 Senn, H. M.; Thiel, S.; Thiel, W., Enzymatic hydroxylation in p-hydroxybenzoate hydroxylase: A case study for QM/MM molecular dynamics. *J. Chem. Theory Comput.* **2005** 1, 494-505.
52 Senn, H. M.; Kaestner, J.; Breidung, J.; Thiel, W., Finite-temperature effects in enzymatic reactions - Insights from QM/MM free-energy simulations. *Can. J. Chem.* **2009** 87, 1322-1337.
53 Dey, A.; Peng, Y.; Broderick, W. E.; Hedman, B.; Hodgson, K. O.; Broderick, J. B.; Solomon, E. I., S K-edge XAS and DFT calculations on SAM dependent pyruvate formate-lyase activating enzyme: nature of interaction between the Fe_4S_4 cluster and SAM and its role in reactivity. *J. Am. Chem. Soc.* **2011** 133, 18656-18662.
54 Blachly, P. G.; Sandala, G. M.; Giammona, D. A.; Liu, T.; Bashford, D.; McCammon, J. A.; Noodleman, L., Use of broken-symmetry density functional theory to characterize the IspH oxidized state: Implications for IspH mechanism and inhibition. *J. Chem. Theory Comput.* **2014** 10, 3871-3884.
55 Blachly, P. G.; Sandala, G. M.; Giammona, D. A.; Bashford, D.; McCammon, J. A.; Noodleman, L., Broken-Symmetry DFT computations for the reaction pathway of IspH, an iron-sulfur enzyme in Pathogenic Bacteria. *Inorg. Chem.* **2015** 54, 6439-6461.
56 Zhao, C.; Li, Y.; Wang, C.; Chen, H., Mechanistic dichotomy in the activation of SAM by radical SAM enzymes: QM/MM modeling deciphers the determinant. *ACS Catal.* **2020** 10, 13245-13250.
57 Beinert, H.; Holm, R. H.; Munck, E., Iron-sulfur clusters: Nature's modular, multipurpose structures. *Science* **1997** 277, 653-659.
58 Noodleman, L.; Peng, C. Y.; Mouusca, J. M.; Case, D. A., Orbital interactions, electron delocalization and spin coipling in iron-sulfur clusters. *Coordin. Chem. Rev.* **1995** 209, 199-244.
59 Dey, A.; Glaser, T.; Couture, M. M. J.; Eltis, L. D.; Holm, R. H.; Hedman, B.; Hodgson, K. O.; Solomon, E. I., Ligand K-Edge X-ray absorption spectroscopy of $[Fe_4S_4]^{1+,2+,3+}$ clusters: Changes

in bonding and electronic relaxation upon redox. *J. Am. Chem. Soc.* **2004** 126, 8320-8328.
60 Sharma, S.; Sivalingam, K.; Neese, F.; Chan, G. K.-L., Low-energy spectrum of iron-sulfur clusters directly from many-particle quantum mechanics. *Nat. Chem.* **2014** 6, 927-933.
61 Noodleman, L.; Lovell, T.; Liu, T. Q.; Himo, F.; Torres, R. A., Insights into properties and energetics of iron-sulfur proteins from simple clusters to nitrogenase. *Curr. Opin. Chem. Biol.* **2002** 6, 259-273.
62 Stiebritz, M. T.; Hiller, C. J.; Sickerman, N. S.; Lee, C. C.; Tanifuji, K.; Ohki, Y.; Hu, Y., Ambient conversion of CO2 to hydrocarbons by biogenic and synthetic Fe_4S_4 clusters. *Nat. Catal.* **2018** 1, 444-451.
63 Pang, H.; Walker, L. M.; Silakov, A.; Zhang, P.; Yang, W.; Elliott, S. J.; Yokoyama, K., Mechanism of reduction of an aminyl radical intermediate in the radical SAM GTP 3',8-Cyclase MoaA. *J. Am. Chem. Soc.* **2021** 143, 13835-13844.
64 Lee, Y.-H.; Hou, X.; Chen, R.; Feng, J.; Liu, X.; Ruszczycky, M. W.; Gao, J.-M.; Wang, B.; Zhou, J.; Liu, H.-W., Radical S-Adenosyl Methionine Enzyme BlsE Catalyzes a Radical-Mediated 1,2-Diol Dehydration during the Biosynthesis of Blasticidin S. *J. Am. Chem. Soc.* **2022** 144, 4478-4486.
65 Feng, J.; Shaik, S.; Wang, B., Spin-regulated electron transfer and exchange-enhanced reactivity in Fe_4S_4-mediated redox reaction of the Dph2 enzyme during the biosynthesis of diphthamide. *Angew. Chem. Int. Ed.* **2021** 60, 20430-20436.
66 Zhou, S.; Wei, W.-J.; Liao, R.-Z., QM/MM Study of the Mechanism of the Noncanonical S-C gamma Bond Scission in S-Adenosylmethionine Catalyzed by the CmnDph2 Radical Enzyme. *Top. Catal.* **2022** 65, 517-527.
67 Jiang, H.; Svensson, O. K. G.; Cao, L.; Ryde, U., Proton Transfer Pathways in Nitrogenase with and without Dissociated S2B. *Angew. Chem. Int. Ed.* **2022** 10.1002/anie.202208544.
68 Siegbahn, P. E. M., The mechanism for nitrogenase including all steps. *Phys. Chem. Chem. Phys.* **2019** 21, 15747-15759.
69 Cao, L.; Ryde, U., What Is the Structure of the E-4 Intermediate in Nitrogenase? *J. Chem. Theory Comput.* **2020** 16, 1936-1952.
70 Liao, R.-Z.; Zhang, J.-X.; Lin, Z.; Siegbahn, P. E. M., Antiferromagnetically coupled Fe8S9 cluster catalyzed acetylene reduction in a nitrogenase-like enzyme DCCPCh: Insights from QM/MM calculations. *J. Catal.* **2021** 398, 67-75.
71 Dong, G.; Cao, L.; Ryde, U., Insight into the reaction mechanism of lipoyl synthase: a QM/MM study. *J. Biol. Inorg. Chem.* **2018** 23, 221-229.
72 Benediktsson, B.; Bjornsson, R., Analysis of the Geometric and Electronic Structure of Spin-Coupled Iron-Sulfur Dimers with Broken-Symmetry DFT: Implications for FeMoco. *J. Chem. Theory Comput.* **2022** 18, 1437-1457.
73 Jafari, S.; Santos, Y. A. T.; Bergmann, J.; Irani, M.; Ryde, U., Benchmark Study of Redox Potential Calculations for Iron-Sulfur Clusters in Proteins. *Inorg. Chem.* **2022** 61, 5991-6007.
74 Mejuto-Zaera, C.; Tzeli, D.; Williams-Young, D.; Tubman, N. M.; Matousek, M.; Brabec, J.; Veis, L.; Xantheas, S. S.; de Jong, W. A., The Effect of Geometry, Spin, and Orbital Optimization in Achieving Accurate, Correlated Results for Iron-Sulfur Cubanes. *J. Chem. Theory Comput.* **2022** 18, 687-702.
75 Li Manni, G.; Dobrautz, W.; Bogdanov, N. A.; Guther, K.; Alavi, A., Resolution of Low-Energy States in Spin-Exchange Transition-Metal Clusters: Case Study of Singlet States in Fe(III)(4)S-4 Cubanes. *J. Phys. Chem. A* **2021** 125, 4727-4740.
76 Dobrautz, W.; Weser, O.; Bogdanov, N. A.; Alavi, A.; Li Manni, G., Spin-Pure Stochastic-CASSCF via GUGA-FCIQMC Applied to Iron-Sulfur Clusters. *J. Chem. Theory Comput.* **2021** 17, 5684-5703.
77 Ji, L.; Wang, C.; Ji, S.; Kepp, K. P.; Paneth, P., Mechanism of cobalamin-mediated reductive dehalogenation of chloroethylenes. *ACS Catal.* **2017** 7, 5294-5307.
78 Heckel, B.; McNeill, K.; Elsner, M., Chlorinated ethene reactivity with Vitamin B12. is governed by cobalamin chloroethylcarbanions as crossroads of competing pathways. *ACS Catal.* **2018** 8, 3054-3066.
79 Ho, M.-C.; Menetret, J.-F.; Tsuruta, H.; Allen, K. N., The origin of the electrostatic perturbation in acetoacetate decarboxylase. *Nature* **2009** 459, 393-397.
80 Shaik, S.; Chen, H.; Janardanan, D., Exchange-enhanced reactivity in bond activation by metal-oxo enzymes and synthetic reagents. *Nat. Chem.* **2011** 3, 19-27.
81 Janardanan, D.; Wang, Y.; Schyman, P.; Que, L., Jr.; Shaik, S., The Fundamental Role of Exchange-Enhanced Reactivity in C-H Activation by S=2 Oxo Iron(IV) Complexes. *Angew. Chem., Int. Ed.* **2010** 49, 3342-3345.
82 Janardanan, D.; Usharani, D.; Shaik, S., The Origins of Dramatic Axial Ligand Effects: Closed-Shell MnVO Complexes Use Exchange-Enhanced Open-Shell States to Mediate Efficient H Abstraction Reactions. *Angew. Chem., Int. Ed.* **2012** 51, 4421-4425.
83 Wang, B.; Wu, P.; Shaik, S., Critical Roles of Exchange and Superexchange Interactions in Dictating Electron Transfer and Reactivity in Metalloenzymes. *J. Phys. Chem. Lett.* **2022** 13, 2871-2877.
84 Neese, F., The ORCA program system. *Wires. Comput. Mol. Sci.* **2012** 2, 73-78.
85 Neese, F., Software update: the ORCA program system, version 4.0. *Wires. Comput. Mol. Sci.* **2018** 8.
86 Neese, F.; Wennmohs, F.; Becker, U.; Riplinger, C., The ORCA quantum chemistry program package. *J. Chem. Phys.* **2020** 152, 224108-224125.
87 Neese, F., Software update: The ORCA program system-Version 5.0. *Wires. Comput. Mol. Sci.* **2022**.
88 Bridwell-Rabb, J.; Zhong, A.; Sun, H. G.; Drennan, C. L.; Liu, H. W., A B12-dependent radical SAM enzyme involved in oxetanocin A biosynthesis. *Nature* **2017** 544, 322-326.
89 Knox, H. L.; Sinner, E. K.; Townsend, C. A.; Boal, A. K.; Booker, S. J., Structure of a B_{12}-dependent radical SAM enzyme in carbapenem biosynthesis. *Nature* **2022** 602, 343-348.
90 Rohac, R.; Amara, P.; Benjdia, A.; Martin, L.; Ruffie, P.; Favier, A.; Berteau, O.; Mouesca, J.-M.; Fontecilla-Camps, J. C.; Nicolet, Y., Carbon-sulfur bond-forming reaction catalysed by the radical SAM enzyme HydE. *Nat. Chem.* **2016** 8, 491-500.
91 Nicolet, Y., Structure–function relationships of radical SAM enzymes. *Nat. Catal.* **2020** 3, 337-350.
92 Besandre, R. A.; Chen, Z.; Davis, I.; Zhang, J.; Ruszczycky, M. W.; Liu, A.; Liu, H.-W., HygY is a twitch radical SAM epimerase with latent dehydrogenase activity revealed upon mutation of a single cysteine residue. *J. Am. Chem. Soc.* **2021** 143, 15152-15158.
93 Amara, P.; Mouesca, J. M.; Bella, M.; Martin, L.; Saragaglia, C.; Gambarelli, S.; Nicolet, Y., Radical *S*-Adenosyl-L-methionine tryptophan lyase (NosL): How the protein controls the carboxyl radical CO_2^- migration. *J. Am. Chem. Soc.* **2018** 140, 16661-16668.
94 Impano, S.; Yang, H.; Shepard, E. M.; Swimley, R.; Pagnier, A.; Broderick, W. E.; Hoffman, B. M.; Broderick, J. B., S-Adenosyl-l-ethionine is a Catalytically Competent Analog of S-Adenosyl-l-methione (SAM) in the Radical SAM Enzyme HydG. *Angew. Chem., Int. Ed.* **2021** 60, 4666-4672.
95 Esakova, O. A.; Grove, T. L.; Yennawar, N. H.; Arcinas, A. J.; Wang, B.; Krebs, C.; Almo, S. C.; Booker, S. J., Structural basis for tRNA methylthiolation by the radical SAM enzyme MiaB. *Nature* **2021** 597, 566-570.

Table of Contents